International Review on Modelling and Simulations (I.RE.MO.S.), Vol. 14, N. 6
ISSN 1974-9821 December 2021

Hydrodynamic Characteristics of Fin Shaped Geometry for Sacrificial Anode Body to Reduce the Hull Appendages Effect

Ahmad Fauzan Zakki[1], Good Rindo[1], Mohd Ridwan[2], Aulia Windyandari[2]

Abstract – *On the previous research, the foil shaped has been proposed to improve the drag force characteristics of the conventional zinc anode as sacrificial cathodic protection. As a part of the previous research efforts, the aim of this research is to evaluate the hydrodynamics characteristics of fin shaped geometry for sacrificial anode body to reduce the hull appendages effects. The configuration of fin shaped geometry has been proposed in order to improve the total drag force that has been generated by the conventional geometry design of the existing sacrificial anodes. The unstructured grid of computational fluid dynamic model has been developed for estimating the total drag force, the drag force coefficient and the flow pattern of the fin shaped geometry. The flow velocity has been defined on the vessel service speed of 5 knots, 8 knots and 10 knots. Comparison with the conventional geometry has been made to measure the influence of the configurations of fin shaped geometry on the total drag force and the drag force coefficient. The results show that the proposed fin shaped geometry has effectively reduced the total drag force of the conventional design.*

Keywords: *Fin Shaped Zinc Anode, Drag Force, Flow Pattern, Sacrificial Anode and Hull Appendages*

Nomenclature

ρ	Density of fluid
C_T	Drag coefficient of sacrificial anode
D	Length of sacrificial anode
H	Height of sacrificial anode
R_T	Total drag resistance
S	Wetted surface area of sacrificial anode
Vol	Volume of sacrificial anode
Vs	Service speed of ship/boat
Vx	Fluid flow velocity in X-axis direction
Vy	Fluid flow velocity in Y-axis direction
Vz	Fluid flow velocity in Z-axis direction
W	Width of sacrificial anode

I. Introduction

During the operational condition, the vessel hull construction is suffering the corrosion problems. Galvanic corrosion has been identified as a major cause of the serious corrosion problem, especially in the stern part of the vessel hull. The adjacent copper material of propeller with the steel material of the vessel hull, which is submerged on the sea water (electrolyte solution), has generated the flow of electric current because of the potential difference of both materials. The principle of cathodic protection using sacrificial anode is providing the galvanic anode, which has potential that is more negative. Therefore, the flow of the electric current is supplied by the potential difference of the sacrificial anode and the protected steel hull. The corrosion protection system using sacrificial anodes on the ship hull can be seen on the Fig. 1. The electrochemical reactions can be described as follows:

- Anodic: $Zn - 2\ e^- \rightarrow Zn^{2+}$;
- Cathodic: $H_2O + ½\ O_2 + 2\ e^- \rightarrow 2\ OH^-$.

Therefore, the cathodic protection on the stern part of the vessel hull requires more pieces of the sacrificial anodes, which is usually made from zinc or aluminum, than the number of anodes in the bow part. However, the body of the sacrificial anode on the hull surface can be identified as an appendage of the vessel hull, which might cause an increase on the resistance performance.

Therefore, the other method has been proposed for the corrosion protection such as the impressed current method.

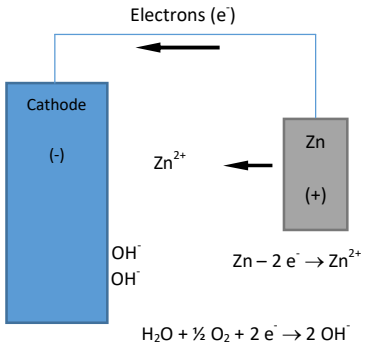

Fig. 1. The principle of sacrificial cathodic protection system on the vessel hull

 https://doi.org/10.15866/iremos.v14i6.20067

Although the impressed current method can eliminate the appendages effect on the vessel hull, the impressed current is relatively more expensive than the sacrificial anode. Meanwhile almost all of the ship building, which is operated in Indonesia, has commonly used the sacrificial anodes than the impressed current systems.

Therefore, the modification of sacrificial anode body that can reduce the appendage effect has become an effective effort to improve the ship resistance performance in Indonesia. On the previous research, the foil shaped geometry has been successfully developed to reduce the drag force which generated by the conventional anodes, [1]. This research is focused on the investigation of the hydrodynamic characteristics of the fin shaped geometry as an effort to reduce the appendages effect due to the installation the sacrificial anode on the hull surface. The configuration of the fin shaped geometry has been developed. The three kinds of fin shaped geometry design have been proposed to be investigated for its influence to reduce the total drag force. The fin shaped with the streamlined body should be capable to improve the drag performance and the optimum ship resistance is obtained on the streamlined optimum hull form. This study initially reviews the previous research on the geometry design development for the improvement of hydrodynamics characteristics such as drag force, pressure drag and flow pattern using computational fluid dynamics. Furthermore, the fin shaped geometry inspired by the dorsal fin has been developed as the body of sacrificial anode to reduce the drag resistance. The performance of the developed fin shaped sacrificial anode has been investigated using the computational fluid dynamics analysis. Finally, the performance comparison between the developed fin shaped and the conventional designs is presented in the final chapter.

II. Literature Review

Several studies have been made through any kind of geometry design development in order to improve and to identify the hydrodynamics characteristics such as vessel hull, submarine, underwater drones, ocean piping, etc.

Most of the research works have adopted the computational fluid dynamic method in order to investigate the hydrodynamics characteristics such as drag force, pressure drag, and flow pattern. Recent study of the CFD application to investigate and to identify the hydrodynamic characteristics of the design modification and development can be found on some literatures.

Prakash and Chandra [2] have implemented the CFD techniques to determine the shallow water resistance of river vessel. The flow pattern around the vessel hull has been modelled included with the free surface effect. The wave pattern simulation has showed general agreement with Havelock theory. The estimated shallow water resistance has shown a good agreement with the empirical method of Schlichting on the sub-critical speeds condition. The CFD method has been concluded as an effective method to predict the resistance performance in the shallow water. Joung et al. [3] have examined the CFD method to predict the drag and propulsion performance of a design concept Underwater Autonomous Vehicle (UAV). The prediction has been made in order to determine the thruster to perform the required service speed of the UAV. The research work has obtained the hydrodynamics forces on the pure heaving and the pure pitching motion. The bollard pull test has been conducted to measure the thruster power. The averaged value of the measured data has been compared with the CFD analysis simulation result. The result has showed that the CFD analysis is reliable to be adopted for the estimation of hydrodynamics characteristics within the initial design phase.

Szelangiewicz and Zelazny [4] have presented the influence of the water flow direction of the vertical pipe of ocean mining system. The CFD analysis has been adopted to model the hydrodynamic force and the torsional moment that have acted on the pipe. The results show that the simulation analysis has a good agreement with the experimental results. It is obtained that there are noticeable vortexes located behind the pipeline. The vortexes have generated the oscillatory movement in the pipeline. The CFD analysis can pronounce the hydrodynamics moment that causes the twisting of the pipelines on the vertical axis. The cylindrical buoyancy module has been proposed in order to avoid the variability of the hydrodynamics force. Mudarisov et al. [5] have presented the methodology of an assessment of soil loosening and compaction process with working tool based on pressure distribution pattern using CFD model.

The geometry parameters of tillage tools and machine have been justified by taking into account the forming conditions. The CFD analysis application on the manufacturing process and mechanical engineering can be found in Espinel et al. [6], which have analyzed the physical phenomena of the two-phase flow with Open FOAM for water jet cutting processes. In another other study, Espinel et al. [7] have studied the performance of NACA 0012 airfoil using Open FOAM. Cardenas et al. [8] have investigated the industrial safety valve subjected to high-pressure values in a virtual environment with open foam. Rojas et al. [9] have presented a parametric study of the centrifugal airfoil fans using CFD analysis.

Abril et al. [10] have studied the combined cycle power plant heat exchanger using CFD analysis. Udaiyakumar et al. [11] have developed contour design and numerical simulation model of aerospike nozzle in order to investigate the truncation effects of nozzle. M. Kosek [12] has developed simulation model and real time diagnostic system of Kaplan turbine rotating union.

Orjuela et al. [13] have adopted CFD in order to determine the mass flow by blow-by in light aircraft diesel engines. Palacios et al. [14] have developed geometry design of receiver pipe to increase transfer surface area and improve thermal efficiency. Arunkumar et al. [15] have investigated the effect of turbulators for the improvement of thermal performance of solar air

heater. Aouimer et al. [16] have investigated flow induced vibrations on marine propellers using CFD analysis. Pathan et al. [17] have optimized the blowing pressure ratio of an enlarged duct. Samara et al. [18] have investigated the performance of two co-axial jets exiting from the base of slender body. Rojas et al. [19] have investigated the characteristics of turbulent flow in the cylinders of a diesel engine. The implementation of the CFD on the estimation hydrodynamics characteristics during the initial design phase also can be found in Elkafas et al. [20], with the prediction of ship resistance using ANSYS-CFX. In Bakica et al. [21] the two benchmark cases (containership KCS and bulk carrier JBC) have been evaluated using OpenFOAM platform. In Olmos et al. [22], the CFD analysis of the submarine take-off and submarine flight of the unmanned vehicle has been conducted. Ganesan and Esakki [23] have minimized the drag characteristics of unmanned amphibious aerial vehicle using the CFD method. In Czyz et al. [24], the CFD method has been adopted for investigating the aerodynamics drag force of the powerboats. Piskur et al. [25] have analyzed the fin drag force of biomimetic underwater vehicle using Incompressible Computational Fluid Dynamics (ICFD) solver of LS-DYNA. Regarding the above conditions, this research has adopted the CFD analysis in order to estimate the hydrodynamic characteristics of the developed fin shaped geometry for the sacrificial anode.

The CFD analysis has been used for the calculation of the drag force generated by the fin shaped anode. A comparison with the conventional model has been presented in order to measure the influence of geometry modification on the drag force performance that provides a contribution on the ship resistance.

III. Material and Methods

III.1. Conceptual Design of the Fin Shaped Geometry

The development of the fin shaped geometry is inspired by the dorsal fin of fish, Fig. 2. Actually, the dorsal fin has a function to keep the fish in the upright position and to stabilize the fish motion on the sudden turns. Otherwise, the dorsal fin should have an efficient drag characteristic in order to support an efficiently impulsive and excellent fish motion. The modification of the geometry of the dorsal fin of sharks has been conducted in order to develop the fin geometry for the sacrificial anode.

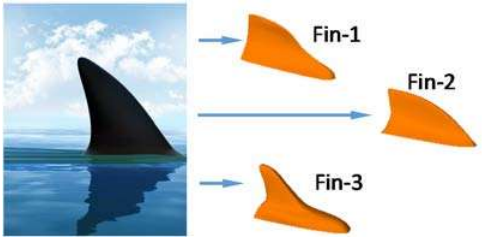

Fig. 2. The geometry of the shark dorsal fin as a parent model of the fin shaped anode

There are three kinds of fin geometry that have been made as follows:

- Fin-1 Type: the fin shaped is started with a slightly concave spline and turns to a convex spline. The end of the fin is a flat plane. The illustration of Fin-1 type geometry can be seen in Figs. 3;
- Fin-2 Type: the fin shaped has a convex spline (an arc line) and the end part is closed with the concave plane. The illustration of Fin-2 type geometry can be seen in Figs. 4;
- Fin-3 Type: the fin shaped is similar to the shark fin with a small part of the shark upper body. The illustration of Fin-3 type geometry can be seen in Figs. 5.

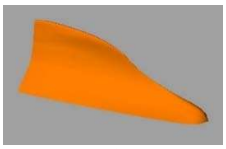

(a)

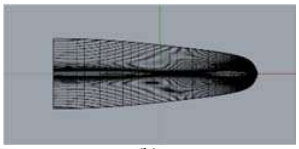

(b)

Figs. 3. Geometry design Fin-1 of zinc anode: (a) perspective view; (b) top view

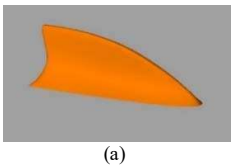

(a)

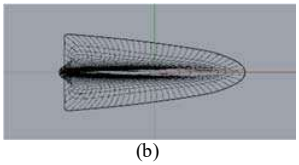

(b)

Figs. 4. Geometry design Fin-2 of zinc anode: (a) perspective view; (b) top view

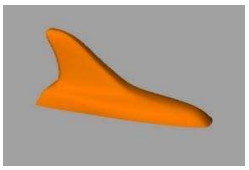

(a)

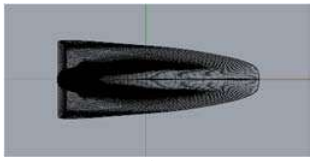

(b)

Figs. 5. Geometry design Fin-3 of zinc anode: (a) perspective view; (b) top view

All the configurations of the fin geometry have similar volume and weight. The size of the principal dimension such as the weight, height and the wetted surface area is presented on Table I. All the fin shapes have a streamline body that can improve the stream flow compared with the conventional design with the rectangle body, Figs. 6.

After that, the investigation of the hydrodynamic characteristic of the developed fin type is conducted with the computational fluid dynamic analysis.

III.2. Simulation Analysis of the Fin Shaped Geometry

The first step of the simulation analysis is preparing the simulation model. Since the simulation uses the finite volume algorithm, the objects of the simulation (the fin body) have been modelled as a void. Otherwise, the fluid domain has been defined as an enclosed prismatic that should be discretized on the set of girds, which is known as a model mesh with many elements. The more complex geometry should be created with the greater number of elements.

Therefore, in order to save the computational time, the simulation model has been run on the half part of the whole model. This simplification can be done because the object of simulation has symmetric body on the centerline (about XZ plane). The tetrahedral elements with the unstructured grid have been selected to model the fluid domain.

As the boundary conditions, the inlet region is determined as the axial upstream of the entry flow, and the outlet region is determined as the downstream of the exit flow.

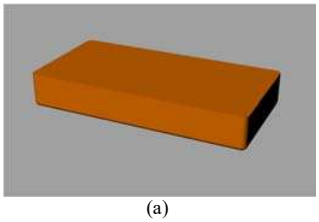

(a)

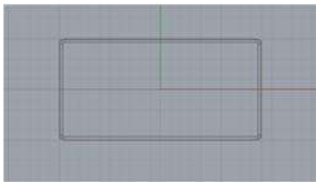

(b)

Figs. 6. Conventional design of zinc anode:
(a) perspective view; (b) top view

TABLE I
THE DESIGN CONFIGURATIONS OF FIN SHAPED ANODE GEOMETRY

Design Parameters	Conventional	Fin-1	Fin-2	Fin-3
Length (*D*) [cm]	20	28.82	26.82	26.21
Height (*T*) [cm]	3	10.36	8.78	10.72
Width (*W*) [cm]	10	9.81	11.20	9.68
Area Surface (*S*) [cm^2]	572.79	509.87	455.21	392.45
Volume (*Vol*) [cm^3]	614	567.2	591.5	594.2

The outlet region location is defined with the distance about the same size of the length of the fin body.

The void model as representation of the fin body is defined and located on one side of the edge of the fluid domain boundary, and it is aligned with the defined fluid flow. The other side of the wall boundary of the simulation model is determined as the defined side flow condition. The detail definition of boundary condition has been presented in Fig. 7 and Table II. The simulation model using the unstructured grid mesh type can be seen in Figs. 8.

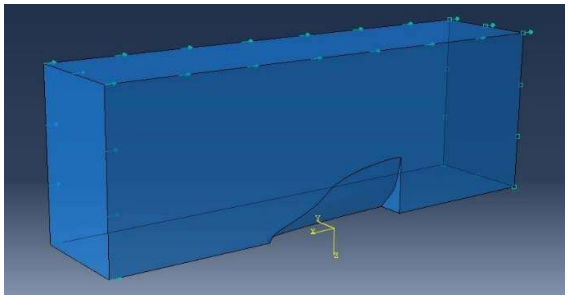

Fig. 7. The illustration of the boundary condition of the CFD analysis

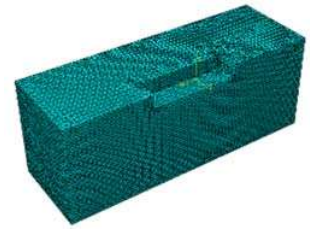

(a)

(b)

(c)

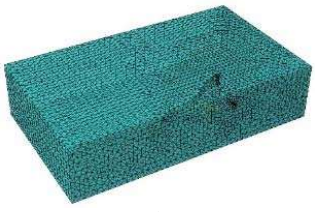

(d)

Figs. 8. Unstructured grid meshing model: (a) Conventional Model; (b) Fin-1 Model; (c) Fin-2 Model; (d) Fin-3 Model

TABLE II
THE BOUNDARY CONDITIONS OF THE CFD MODEL

Defined Boundary	Boundary Type	*Vx*	*Vy*	*Vz*
Fin Surface	Fluid wall condition/No slip	0	0	0
Bottom Flow	Fluid inlet/outlet	Free	Free	0
Inlet Flow	Fluid inlet/outlet	*-Vs*	0	0
Side Flow	Fluid inlet/outlet	Free	0	Free
Top Flow	Fluid inlet/outlet	*-Vs*	0	0
Out Flow	Fluid inlet/outlet	Zero Pressure		

IV. Results and Discussion

IV.1. The Pressure Distribution on the Fin Shaped Bodies

The CFD simulation has been run on the four kinds of geometry, which include conventional, Fin-1, Fin-2 and Fin-3. In the present case, the geometry model has been evaluated on service speed conditions of 5 knot, 8 knot and 10 knot. The CFD analysis uses the Reynold Averaged Navier Stokes (RANS) approach in order to calculate the fluid dynamics behavior on the proposed geometry design. According to the simulation result, it is obtained that the maximum pressure drag of 3517 Pa has been shown by the conventional design on the service speed of 5 knot, Fig. 9(a). All the fin bodies have presented a lower maximum pressure drag than the conventional one. It is indicated that the submerged body shape geometry has significant influence on the generated pressure drag. Furthermore, it can be seen that the application of a streamline body (the fin bodies), on the service speed of 5 knot, has shown a significant reduction of the maximum pressure drag on the conventional sacrificial anode body. The maximum pressure drag of the developed fin bodies are 1754 Pa, 1473 Pa, and 1757 Pa, for the Fin-1 type, Fin-2 type, and Fin-3 type, respectively. All the maximum pressure drags have occurred on the front tip of the bodies. This condition is theoretically accepted because the maximum pressure drag has always occurred on the stagnation point, which is commonly located on the front point.

Amongst the developed fin bodies, it can be seen that Fin-2 type has a smallest maximum pressure drag than the others. It can be explained that the Fin-2 type has a better shape to distribute the fluid flow. Therefore, the concentration pressure drag on the stagnation point can be distributed appropriately. The illustration of the pressure drag distribution can be seen in Figs. 9.

IV.2. The Velocity Distribution and Flow Pattern on the Fin Shaped Bodies

Figures 10 present the velocity distribution of the fluid flow on the service speed 5 knot (2.572 m/s). Compared with the fin bodies, the conventional one has generated the larger maximum flow velocity. It is indicated that the conventional body has increased the potential energy of the fluid flow on the adjacent region of the stagnation point, Fig. 10(a).

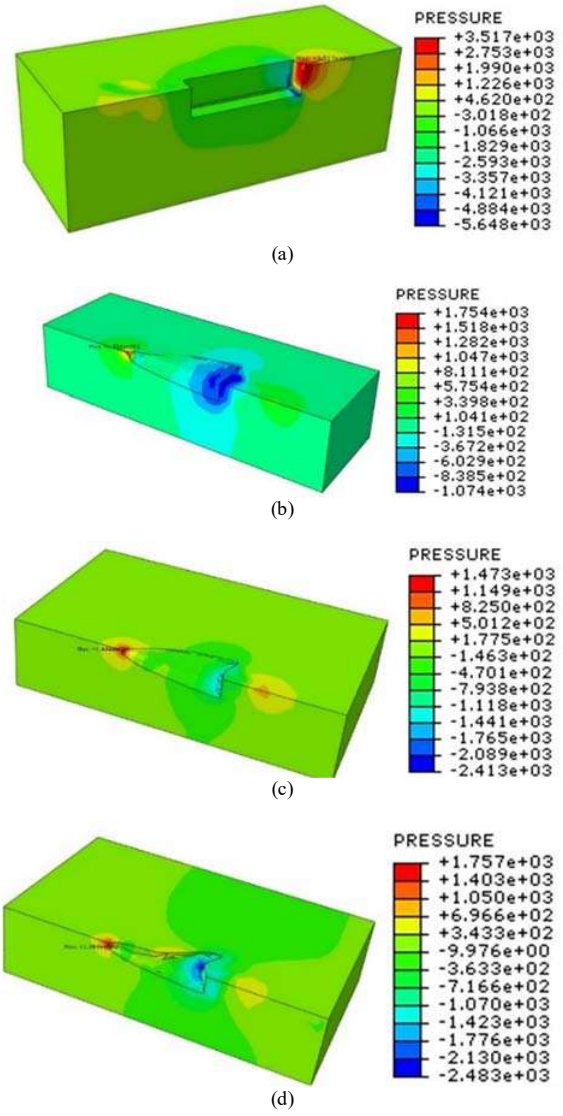

Figs. 9. The pressure distribution in 5 knots:
(a) Conventional; (b) Fin-1; (c) Fin-2; (d) Fin-3

Furthermore, the potential energy has been transformed to kinetic energy when the fluid has been successfully passed/flowed on the body shape barrier.

The larger potential energy have released the larger velocity that generates the greater flow kinetic energy.

Therefore, it can be seen that the location of maximum flow velocity represents the maximum kinetic energy achieved by the fluid flow. Then the maximum velocity has gradually decreased and should be returned to the initial velocity (2.572 m/s). Otherwise, the zero velocity of the fluid flow can be found on the all of end part of the evaluated body. It can be explained that some of the fluid flows have lost their kinetic energy sooner than the other due to the friction with the evaluated body, between the fluid and the sudden change of the end part shape. On the backward side, the laminar fluid flows could lost the kinetic energy and turned in to the eddy flows that could increase the vessel total resistance.

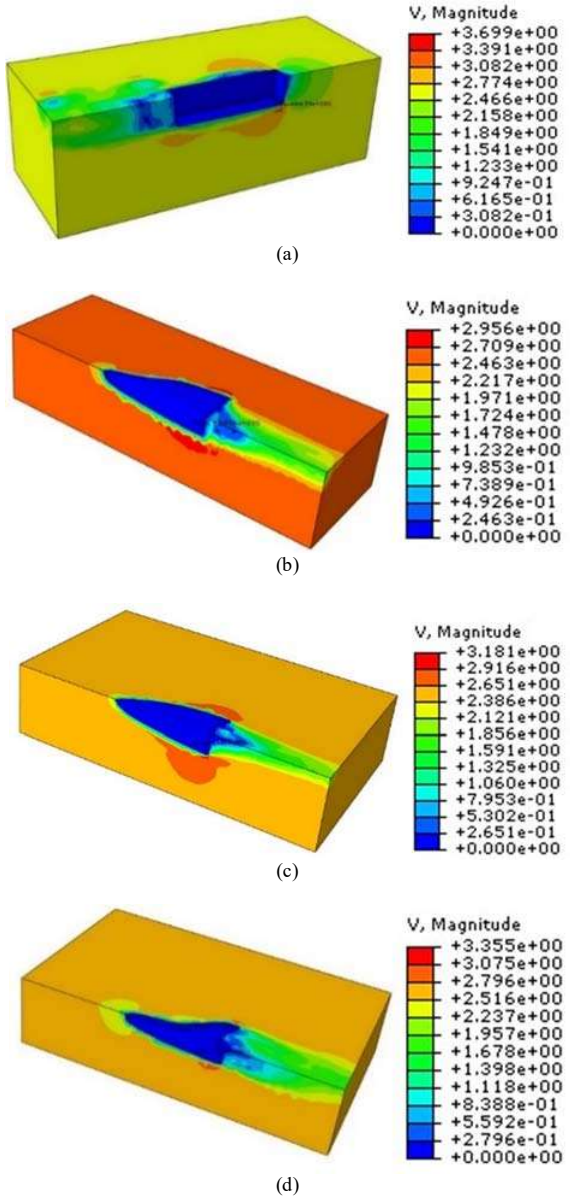

Figs. 10. The velocity distribution in 5 knot: (a) Conventional; (b) Fin-1; (c) Fin-2; (d) Fin-3

Regarding the condition above, Figures 11 present the flow pattern generated by the influence of the evaluated bodies. The fluid flow pattern on the conventional body is presented in Fig. 11(a). The velocity flow has started decreasing right in front of the conventional body. Furthermore, the separation in flow also can be seen on the side part of the body. However, this condition cannot be found on the fin bodies, Figs. 11(b)-(d). In the end part, the eddy flow pattern has significantly occurred on the conventional body. The Fin-3 type has also presented a larger flow separation on the end part, compared with the Fin-1 type and Fin-2 type. It is indicated that Fin-1 and Fin-2 have better geometry shape that can significantly reduce the appendages effect on the resistance performance.

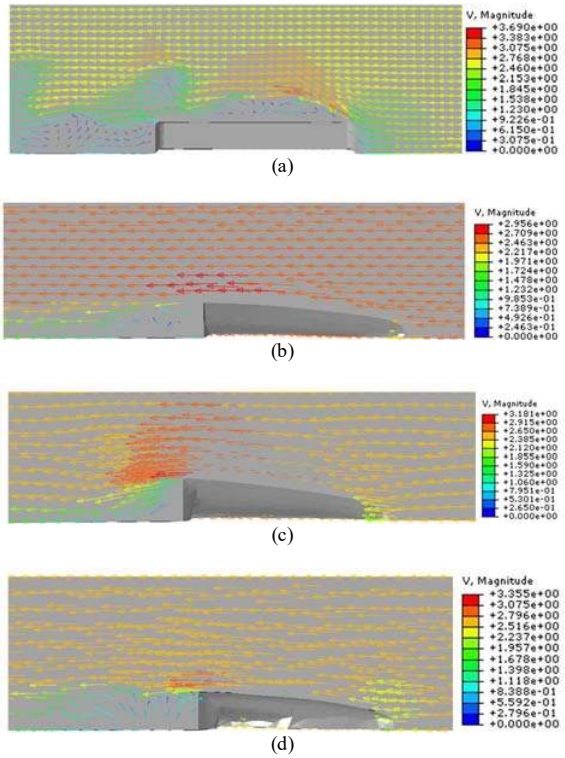

Figs. 11. The flow pattern in 5 knots:
(a) Conventional; (b) Fin-1; (c) Fin-2; (d) Fin-3

IV.3. The Drag Force on the Fin Shaped Bodies

Finally, the CFD simulation has presented the drag force generated by the evaluated bodies. The calculation of the drag force is made through an integration of the pressure drag, which is acted on the surface of the submerged body. Therefore, the submerged body surface is the domain of pressure drag integration in every simulation time step. Figures 12 have presented the magnitude of the drag force as a result of numerical calculation within the simulation time. The drag force behavior on the defined service, which includes 5 knots, 8 knots and 10 knots, has been presented in Figs. 12(a)-(c). According to the simulation results, it can be seen that the generated drag force is fluctuated within the time step. On the initial simulation time, the results have presented a very high value of the drag force. This condition is normal because the initial time is identified as the warm up period (transient state) during the simulation analysis. It can be seen that the diminishing slope has been recognized in the simulation time below 0.34 second. The transitional zone has been defined to ensure that the warm up period is completely ended.

Therefore, the simulation analysis that represents the drag force characteristics have been collected from the selected zone, which is located on the simulation time > 0.5 second. Figures 12 present that all the developed fin bodies have successfully reduced the drag force of the conventional, especially for the Fin-1 type and the Fin-2 type.

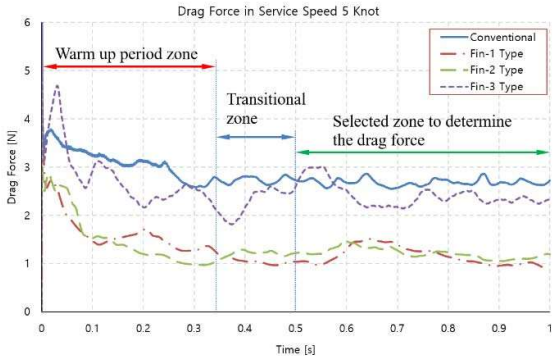

(a)

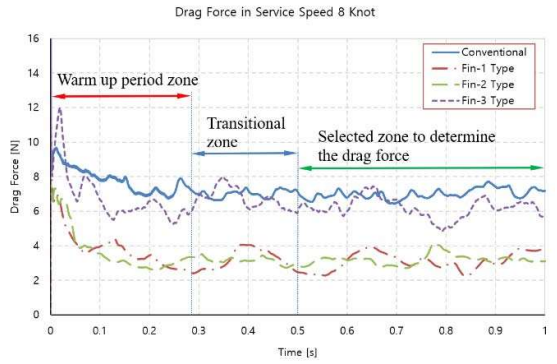

(b)

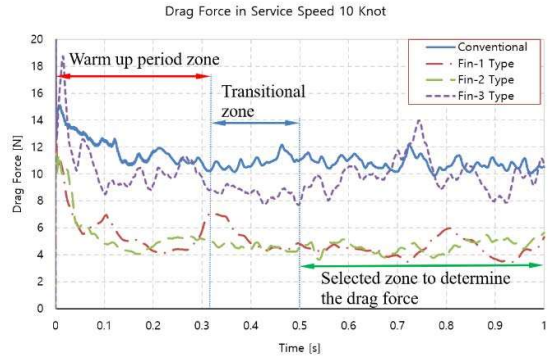

(c)

Figs. 12. The drag force of the fin shaped bodies: (a) 5 knot; (b) 8 knot; (c) 10 knot

However, in the case of the Fin-3 type, the generated drag force is slightly lower than the conventional one.

Moreover, it can be found out that the Fin-3 type has a larger drag force than the conventional because of the fluctuation results. As regard to eliminate the influence of warm up period, the calculation of drag force coefficient has been conducted with the magnitude of drag force on the simulation time > 0.5 s. The drag force has been determined as the middle value of the fluctuated number during the interval. Therefore, at first, the minimum drags force and the maximum drag force should be identified then the magnitude drag force can be determined as the half value of the summation of the maximum and the minimum drag value. The drag coefficient has been determined using the equation of total drag resistance, Eq. (1):

$$C_T = R_T / \left(0.5\rho S V s^2\right) \quad (1)$$

By following the results in Tables III-V, it has been showed that Fin-1 type and Fin-2 type have the smaller drag coefficient than the conventional. The drag coefficient of Fin-1 type is estimated as large as 0.015, and the Fin-2 type is about 0.016. Otherwise, the conventional has shown that the estimated drag coefficient is about 0.028. It can be said that the Fin-1 type and Fin-2 type have reduced the drag coefficient of the conventional as large as 46.43% and 42.86%, respectively. Although the Fin-3 type has generated a slightly lower drag force than the conventional, the drag force coefficient of the body has presented a larger value than the conventional one. This condition might be occurred because the wetted surface area of the Fin-3 type is smaller than the conventional. It is indicated that the generated lower drag of the Fin-3 is caused by the lower wetted surface area not because of the proposed geometry of the fin body. It can be concluded that the geometry of Fin-3 type does not significantly improve the appendages effect on the total resistance performance.

TABLE III
THE DRAG FORCE AND THE DRAG COEFFICIENT OF FIN SHAPE ZINC ANODE IN 5 KNOTS

Model	Min Drag Force > 0.5 s	Max Drag Force > 0.5 s	Drag Force	Wetted Surface Area	Drag Coef. in 5 Knots
Conventional	2.5502	2.863	2.707	0.0286	0.0279
Fin-1	0.9374	1.515	1.226	0.0255	0.0141
Fin-2	1.0562	1.489	1.273	0.0228	0.0164
Fin-3	2.1375	3.021	2.579	0.0196	0.0387

TABLE IV
THE DRAG FORCE AND THE DRAG COEFFICIENT OF FIN SHAPE ZINC ANODE IN 8 KNOTS

Model	Min Drag Force > 0.5 s	Max Drag Force > 0.5 s	Drag Force	Wetted Surface Area	Drag Coef. in 8 Knots
Conventional	6.538	7.377	6.957	0.0286	0.0280
Fin-1	2.277	4.055	3.166	0.0255	0.0143
Fin-2	2.724	3.437	3.081	0.0228	0.0156
Fin-3	5.716	8.002	6.859	0.0196	0.0403

TABLE V
THE DRAG FORCE AND THE DRAG COEFFICIENT OF FIN SHAPE ZINC ANODE IN 10 KNOTS

Model	Min Drag Force > 0.5 s	Max Drag Force > 0.5 s	Drag Force	Wetted Surface Area	Drag Coef. in 10 Knots
Conventional	10.156	12.178	11.167	0.0286	0.0287
Fin-1	4.324	7.131	5.728	0.0255	0.0166
Fin-2	4.230	5.352	4.791	0.0228	0.0155
Fin-3	7.706	11.337	9.522	0.0196	0.0358

V. Conclusion

The developments of the fin shaped geometry to reduce the appendages effect of the sacrificial anode

body on the vessel resistance have been made. The estimation of hydrodynamics characteristics of the fin bodies using the CFD analysis has been also successfully conducted. According to the analysis result, it can be seen that the fin shaped geometry has provided an improvement through the reduction of the drag force, which is generated by the conventional design. The streamline body of the fin geometry has improved the fluid flow pattern when is passing the sacrificial anode body. Consequently, the maximum flow velocity and the pressure drag are decreased. As regard to the flow pattern, it can be found out that the fin bodies have successfully eliminated the flow separation, which is located on the side of the conventional body. The eddy flow on the end of the conventional body is also significantly reduced by the Fin-1 type and the Fin-2 type. However, the eddy flow can still be found on all the developed fin geometries. The cutting body section of the end part of the fin body has been predicted as the source of the eddy flow incidence. Although all the fin bodies have decreased the magnitude of the drag force, only the Fin-1 type and Fin-2 type have smaller drag coefficient than the conventional. It can be concluded that both fin bodies have successfully decreased the drag force through the improvement of the geometry of body shaped. Therefore, it is recommended to implement the both geometry as the shaped of sacrificial anodes.

Otherwise, an experimental study and the investigation of the drag force characteristics of the fin shape installed in a tandem or a special formation of sacrificial anodes position have been suggested for future research.

Acknowledgements

This work was funded by the Directorate of Research and Public Service 2020, through the Higher Education Excellent Fundamental Research Scheme-2020 (Penelitian Dasar Unggulan Perguruan Tinggi, PDUPT-2020).

References

[1] Zakki, A., Rindo, G., Ridwan, M., Alam, B., Numerical Investigation of Hydrodynamic Behavior of Foil Shaped Zinc Anode for Reducing the Hull Appendages Effect, (2020) *International Review of Mechanical Engineering (IREME)*, 14 (7), pp. 477-484. doi: https://doi.org/10.15866/ireme.v14i7.18228

[2] S.M.N. Prakash, B. Chandra, Numerical Estimation of Shallow Water Resistance of a River-Sea Ship using CFD. *International Journal of Computer Applications,* Vol. 71, No. 5, pp. 34-40, 2013.

[3] T.H. Joung, H.S. Choi, S.K. Jung, S.K., K. Sammut, F. He, Verification of CFD analysis methods for predicting the drag force and thrust power of an underwater disk robot. *Int. J. Nav. Archit. Ocean Eng.,* Vol. 6, pp. 269-281, 2014.

[4] T. Szelangiewicz, K. Zelazny, Numerical simulations of water flow around ocean mining piping. *Scientific Journals of the Maritime University of Szczecin,* Vol. 51, pp. 101-108, 2017.

[5] Mudarisov, S., Farkhutdinov, I., Mukhametdinov, A., Aminov, R., Bagautdinov, R., Gallyamov, F., Evaluation of Loosening and Soil Compaction with a Working Tool of Tillage Machines Using a Hydrodynamic Model, (2020) *International Review on Modelling and Simulations (IREMOS)*, 13 (6), pp. 394-399. doi: https://doi.org/10.15866/iremos.v13i6.19224

[6] Espinel, E., Rojas, J., Florez, E., 2D Simulation of Two-Phase Flow for Water Jet Cutting Processes with OpenFOAM®, (2021) *International Review on Modelling and Simulations (IREMOS)*, 14 (4), pp. 301-310. doi: https://doi.org/10.15866/iremos.v14i4.19332

[7] Espinel, E., Rojas, J., Florez Solano, E., Computational Fluid Dynamics Study of NACA 0012 Airfoil Performance with OpenFOAM®, (2021) *International Review of Aerospace Engineering (IREASE)*, 14 (4), pp. 201-210. doi: https://doi.org/10.15866/irease.v14i4.19348

[8] Cardenas, J., Pabón, J., Rojas, J., CFD Study of Industrial Safety Valves in a Virtual Environment with OpenFOAM® Software, (2020) *International Review of Mechanical Engineering (IREME)*, 14 (11), pp. 674-683. doi: https://doi.org/10.15866/ireme.v14i11.19031

[9] Rojas, J., Espinel, E., Florez, E., Parametrical Study of Centrifugal Airfoil Fans by Computational Tools, (2020) *International Review of Mechanical Engineering (IREME)*, 14 (12), pp. 750-759. doi: https://doi.org/10.15866/ireme.v14i12.19281

[10] Orjuela Abril, S., Acevedo, C., Cardenas Gutierrez, J., Computational Fluid Dynamics Analysis of Combined Cycle Power Plant Heat Exchanger with OpenFOAM® Software, (2020) *International Review on Modelling and Simulations (IREMOS)*, 13 (5), pp. 319-328. doi: https://doi.org/10.15866/iremos.v13i5.18891

[11] Udaiyakumar, K., Iyer, K., Akhil, V., Motwani, A., Bhaise, V., Numerical Simulation and Contour Design of Aerospike Nozzle: a Behavioural Study on Truncation Effects of Nozzle, (2020) *International Review of Aerospace Engineering (IREASE)*, 13 (4), pp. 141-149. doi: https://doi.org/10.15866/irease.v13i4.17343

[12] Kosek, M., CFD Simulation of Kaplan Turbine Rotating Union and the Development of a Real Time Diagnostic System, (2021) *International Review on Modelling and Simulations (IREMOS)*, 14 (5), pp. 311-325. doi: https://doi.org/10.15866/iremos.v14i5.21217

[13] Orjuela, S., Valencia, G., Duarte Forero, J., Computational Fluid Dynamics Study of Blow-By in Light Aircraft Diesel Engines, (2020) *International Review of Aerospace Engineering (IREASE)*, 13 (6), pp. 208-216. doi: https://doi.org/10.15866/irease.v13i6.18586

[14] Palacios, A., Amaya, D., Ramos, O., Thermal Analysis of a Parabolic Trough Collectors with Cylindrical and Fractal Receiver Under Serial-Parallel Configuration, (2021) *International Journal on Energy Conversion (IRECON)*, 9 (4), pp. 140-155. doi: https://doi.org/10.15866/irecon.v9i4.19563

[15] Arunkumar, H., Karanth, K., Sharma, N., Madhwesh, N., CFD Analysis on Rectangular Shaped Variable Height Turbulators Fitted in a Solar Air Heater for Improved Thermal Performance, (2021) *International Review on Modelling and Simulations (IREMOS)*, 14 (3), pp. 204-212. doi: https://doi.org/10.15866/iremos.v14i3.19939

[16] Aouimer, Y., Boutchicha, D., Hamoudi, B., Numerical and Experimental Study of Fluid-Structure Interaction of a Marine Propeller, (2020) *International Review of Mechanical Engineering (IREME)*, 14 (5), pp. 282-289. doi: https://doi.org/10.15866/ireme.v14i5.17582

[17] Pathan, K., Dabeer, P., Khan, S., An Investigation to Control Base Pressure in Suddenly Expanded Flows, (2018) *International Review of Aerospace Engineering (IREASE)*, 11 (4), pp. 162-169. doi: https://doi.org/10.15866/irease.v11i4.14675

[18] Samara, M., Vashishtha, A., Watanabe, Y., Suzuki, K., Flow-Field and Performance Study of Coaxial Supersonic Nozzles Operating in Hypersonic Environment, (2020) *International Review of Aerospace Engineering (IREASE)*, 13 (1), pp. 25-39. doi: https://doi.org/10.15866/irease.v13i1.18282

[19] Rojas, J., Valencia Ochoa, G., Duarte Forero, J., CFD Analysis of Swirl Effect in a Diesel Engine Using OpenFOAM, (2020) *International Review on Modelling and Simulations (IREMOS)*, 13 (1), pp. 8-15.

doi: https://doi.org/10.15866/iremos.v13i1.18372
[20] A.G. Elkafas, M.M. Elgohary, A.E. Zeid, Numerical study on the hydrodynamic drag force of a container ship model. *Alexandria Engineering Journal,* Vol. 58, pp. 849–859, 2019.
[21] A. Bakica, I. Gatin, V. Vukcevic, H. Jasak, N. Vladimir, Accurate assessment of ship-propulsion characteristics using CFD. *Ocean Engineering,* vol. 175, pp. 149–162, 2019.
[22] S. Olmos, J. De Lara, P. Carrasco, Investigation of hydrodynamic lift and drag on an autonomous winged submarine using computational fluid dynamics. *Ocean Engineering.* Vol. 186, 106094, 2019.
[23] S. Ganesan, B. Esakki, Computational fluid dynamic analysis of an unmanned amphibious aerial vehicle for drag reduction. *International Journal of Intelligent Unmanned Systems* Vol. 8 No. 3, pp. 187-200, 2020.
[24] Z. Czyz, P. Karpinski, C. Boujelbene, Investigation of the Aerodynamic Drag Force Exerted on a Powerboat. *Advances in Science and Technology Research Journal.* Vol. 14, Issue 3, pp.141–148, 2020.
[25] P. Pizkur, P. Szymak, L. Flis, J. Sznajder, Analysis of a Fin Drag Force in a Biomimetic Underwater Vehicle. *Naše more.* Vol. 67, No. 3, pp. 192-198, 2020.

Authors' information

[1]Naval Architecture Department, Engineering Faculty, Diponegoro University, Semarang, 50275, Indonesia.

[2]Industrial Technology Department, Vocational School, Diponegoro University, Semarang, 50275, Indonesia.

Dr. **Ahmad Fauzan Zakki** was born in 1975, at Surabaya City, East Java, Indonesia. He received a doctoral degree in naval architecture and marine systems engineering at Pukyong National University, Busan, South Korea. Currently, he works at the Department of Naval Architecture, Faculty of Engineering, Diponegoro University. His research interests are ship design, structure, and finite element analysis.

Good Rindo was born in 1988, at Jambi City, Jambi, Indonesia. He received a master's degree in Marine Technology Post Graduate Program, Institute Technology of Sepuluh Nopember, Indonesia. Currently, he works at the Department of Naval Architecture, Faculty of Engineering, Diponegoro University. His research interests are hull form design and computational fluid dynamics analysis.

Dr. **Mohd Ridwan** was born in 1970, at Bukit Tinggi City, West Sumatra, Indonesia. He received a doctoral degree in Coastal Resources Management, Faculty of Fishery and Marine Science, Diponegoro University. Currently, he works at the Department of Industrial Technology, School of Vocation, Diponegoro University. His research interests are ship production engineering and ship production,

Aulia Windyandari was born in 1977, at Probolinggo City, East Java, Indonesia. She received Master degree of marine systems and control engineering in Sepuluh Nopember Institute of Technology, Surabaya, Indonesia. Currently, she works at the Department of Industrial Technology, School of Vocation, Diponegoro University. Her research interests are marine system and control design and composites material for marine used.

